Spectrochimica Acta Part A: Molecular and Biomolecular Spectroscopy 243 (2020) 118797

Contents lists available at ScienceDirect

Spectrochimica Acta Part A: Molecular and Biomolecular Spectroscopy

journal homepage: www.elsevier.com/locate/saa

A dual-functional fluorescent probe for sequential determination of Cu^{2+}/S^{2-} and its applications in biological systems

Xiao-Jing Yan [a], Zhi-Gang Wang [a], Yang Wang [a], Yu-Ying Huang [a], Hai-Bo Liu [b,*], Cheng-Zhi Xie [a,c,**], Qing-Zhong Li [d], Jing-Yuan Xu [a,*]

[a] Department of Chemical Biology and Tianjin Key Laboratory on Technologies Enabling Development of Clinical Therapeutics and Diagnostics, School of Pharmacy, Tianjin Medical University, Tianjin 300070, PR China
[b] Institute of Medicinal Plant Development, Chinese Academy of Medical Sciences, Peking Union Medical College, Beijing 100193, PR China
[c] Key Laboratory of Advanced Energy Materials Chemistry (Ministry of Education), Nankai University, Tianjin 300071, PR China
[d] The Laboratory of Theoretical and Computational Chemistry, School of Chemistry and Chemical Engineering, Yantai University, Yantai 264005, PR China

ARTICLE INFO

Article history:
Received 4 June 2020
Received in revised form 19 July 2020
Accepted 21 July 2020
Available online 06 August 2020

Keywords:
Fluorescent probe
Cu^{2+}/S^{2-}
Practical application
DFT calculation
ON-OFF-ON

ABSTRACT

A new acylhydrazine-derived Schiff base fluorescence probe DMI based on "ON-OFF-ON" fluorescence strategy was presented in this paper. Probe DMI could detect Cu^{2+} selectively and sensitively with dramatic fluorescence quenching in CH_3OH-PBS (v/v = 3:7) mixed solution. Once the complex DMI-Cu^{2+} interacted with S^{2-}, 10.67-folds fluorescence increase was induced via a displacement mechanism under the same experimental conditions. The corresponding detection limits for Cu^{2+} and S^{2-} were calculated to be 1.52×10^{-8} M and 1.79×10^{-8} M, respectively. The structures of DMI and DMI-Cu^{2+} were systematically characterized by Job's plot analysis, ESI-MS, IR, X-ray diffraction and density functional theory calculations. Furthermore, fluorescence imaging in MCF-7 cells and zebrafish demonstrated the probe DMI could act as a useful tool to monitor and track intracellular Cu^{2+} and S^{2-}, which was encouraged by remarkable fluorescence performance and low cytotoxicity. Importantly, the complex DMI-Cu^{2+} could be applied to detect corrupt blood samples, which could estimate the time of death.

1. Introduction

Copper is one of the most sufficient and essential trace elements in human body and takes part in a variety of fundamental biological and physiological processes [1–3]. The concentration of copper ion in the cell is closely related with human health [4]. Abnormal level of copper ion may break the dynamic balance of numerous substances in the body [5], which is connected with many neurodegenerative diseases, including amyotrophic lateral sclerosis [6,7], Parkinson's [8], Alzheimer's [9,10], and prion diseases [11]. At the same time, copper ion, as a heavy metal ion, may produce potentially toxic pollutants to the environment and exert irreversible threat to the global sustainable development [12,13]. Similarly, hydrogen sulfide (H_2S), as a hazardous gas with a smell of rotten eggs, is not only from industrial processes but also from organic matter corruption processes [14–16]. Sulfide can quickly hydrolyze to H_2S and HS^- at physiological pH, which have higher toxicity than sulfide itself [17–19]. Meanwhile, as a vital gaseous signal molecule in living organisms, H_2S plays crucial roles in the nervous system and metabolic system [20]. However, continuous exposure to inappropriate level of H_2S can damage respiratory, disrupt the normal function of human body and cause a range of sever diseases like Down's syndrome, hypertension, diabetes, and liver cirrhosis [21–25]. Hence, it is highly desired to develop an efficient and sensitive way for motoring copper ion and H_2S in environmental and biological systems.

Numerous fluorescence probes have been established to detect H_2S and most of them are based on the following mechanisms: displacement method based on the strong affinity of S^{2-} to Cu^{2+} [26,27], azide reduction [28,29] and nucleophilic reaction [30]. Many of these probes have drawbacks of high toxicity, long response time and rigid reaction conditions [31–33]. However, reversible detection according to the first strategy has attracted increasing attention [34]. On the one hand, Cu^{2+} has an incompletely filled d-orbital which provides an opportunity for quenching fluorescence [35,36]. On the other hand, the reaction of S^{2-} and Cu^{2+} forms a stable compound CuS with lower solubility (CuS: $K_{sp} = 6.36 \times 10^{-36}$) than common Cu^{2+}-probe complexes [37,38]. These two favorable factors make possibilities to turn fluorescence off and on. Recently, several fluorescent probes have

* Corresponding authors.
** Correspondence to: C.-Z. Xie, Department of Chemical Biology and Tianjin Key Laboratory on Technologies Enabling Development of Clinical Therapeutics and Diagnostics, School of Pharmacy, Tianjin Medical University, Tianjin 300070, PR China.
E-mail addresses: hbliu@implad.ac.cn (H.-B. Liu), xiechengzhi@tmu.edu.cn (C.-Z. Xie), xujingyuan@tmu.edu.cn (J.-Y. Xu).

https://doi.org/10.1016/j.saa.2020.118797
1386-1425/

been designed and synthesized to sequentially detect Cu^{2+} and S^{2-} via "ON-OFF-ON" strategy [39,40]. The mechanism is regarded as a copper sulfide precipitation strategy which can recover the fluorescence response of free probes [41]. Nevertheless, few probes have good biocompatibility and water-solubility, which limit their applications in biological research [42,43]. Thus, developing a novel fluorescent probe with excellent performance is highly important and indispensable.

It is an efficient way to design fluorescent probes based on selective combination of fluorescent groups and auxiliary groups [44,45]. Coumarin compounds and its derivatives have excellent fluorescence performance of good optical properties and biocompatibility [46–49]. Due to containing the C═O and C═N functional group, the acylhydrazine Schiff base compounds can provide an appropriate binding environment to recognize target ions [50,51]. Herein, according to the above strategies and as a continuation of our research work about "ON-OFF-ON" fluorescence detection [52,53], we developed a novel acylhydrazine-derived Schiff base receptor N′-((7-(diethylamino)-2-oxo-2H-chromen-3-yl) methylene) isoquinoline-1-carbohydrazide (DMI) with the reaction of 7-(diethylamino)-2-oxo-2H-chromene-3-carbaldehyde and isoquinoline-1-carbohydrazide. The probe DMI could specifically detect Cu^{2+} with dramatic fluorescence quenching in CH_3OH-PBS (v/v = 3:7) buffer solution. Further studies indicated that the complex DMI-Cu^{2+} could act as a probe to monitor H_2S by UV–Vis and fluorescence spectra. Meanwhile, DMI and DMI-Cu^{2+} could be applied in the fluorescence imaging in cells and zebrafish. In addition, the detection of real samples could also be achieved.

2. Experimental section

2.1. Synthesis of probe DMI

The synthetic procedure of probe DMI was displayed in Scheme 1. Noline-1-carbohydrazide [54] and 7-(diethylamino)-2-oxo-2H-chromene-3-carbaldehyde [55] were synthesized based on the previously reported route. Isoquinoline-1-carbohydrazide (374 mg, 2 mmol) was dissolved in 25 mL methanol solution, and 5 mL anhydrous methanol solution of 7-(diethylamino)-2-oxo-2H-chromene-3-carbaldehyde (490 mg, 2 mmol) was added gradually with stirring. The mixed solution was refluxed for 5 h under stirring, which was monitored by TLC. When the reaction finished, the mixture was cooled to room temperature. The precipitate was collected by filtration and washed with methanol three times. Ultimately, an orange solid DMI was obtained through drying under vacuum. Yield: 600.5 mg, 72.5%. ^{1}H NMR (400 MHz, DMSO-d_6): δ (ppm): 12.33 (1H, s, NH), 8.78 (1H, d, ArH), 8.60 (1H, d, ArH), 8.52 (1H, s, =CH), 8.43 (1H, s, ArH), 6.58 (1H, s, ArH), 3.49–3.45 (4H, q, CH_2), 1.17–1.12 (6H, t, CH_3) (Fig. S1). ^{13}C NMR (101 MHz, DMSO-d_6): δ (ppm): 167.3, 166.9, 161.8, 156.6, 152.3, 148.5, 146.2, 144.2, 141.6, 136.1, 133.9, 132.4, 131.3, 130.8, 128.8, 117.7, 114.4, 113.3, 110.3, 101.6, 49.4, 17.5 (Fig. S2). ESI-MS (*m*/*z*) calculated $[DMI + H]^+$ = 415.2, found 415.5, $[DMI + Na]^+$ = 437.2, found 437.5 (Fig. S3). IR (KBr cm^{-1}): υ(C=O):1678.2, υ(Schiff-base) C=N: 1617.7 (Fig. S4).

2.2. Optical measurement

The probe DMI was dissolved in DMF to obtain the stock solution (1 mM). Stock solutions of various ions (Na^+, K^+, Ca^{2+}, Fe^{3+}, Zn^{2+}, Mg^{2+}, Al^{3+}, Cd^{2+}, Cu^{2+}, Co^{2+}, Ni^{2+}, Br^-, CH_3COO^-, Cl^-, F^-, $H_2PO_4^-$, HPO_4^{2-}, HSO_3^-, NO_2^-, NO_3^-) were prepared from their corresponding nitrate salts and sodium salts in methanol solution, respectively. The solution of S^{2-} was prepared from Na_2S. All UV–vis and fluorescence experiments were performed in CH_3OH-PBS (2 mL, v/v = 3:7) buffer solution at room temperature. The titration experiments were operated by gradually incremental additions of stock solutions (Cu^{2+}/S^{2-}) to DMI or DMI-Cu^{2+} solution. Job's plot experiment is an effective way to determine the coordination ratio of probe with metal ions, which was obtained by recording absorbance with steadily concentration ratio changes. All the measurements were carried out less than 1 min after mixing thoroughly.

2.3. X-ray crystallography

The crystal structure of DMI was displayed in Fig. 1. X-ray data collection and structural determination were provided in the Supporting Information. The crystallographic data for DMI were listed in Table S1. Selected bond lengths and bond angles were listed in Table S2 and S3. Structural information of DMI had been deposited at the Cambridge Crystallographic Data Center (CCDC 2000671).

2.4. Calculation studies

The density functional theory (DFT) calculation of probe DMI and its complex were performed on the Gaussian 09 program using Becke-3-Lee-Yang-Parr exchange function (B3LYP). The basis set LANL2DZ and 6-31+G(d,p) had been employed to Cu^{2+} and C, H, N, O, respectively, and the optimized structure of DMI and its Cu complex were obtained [56–59].

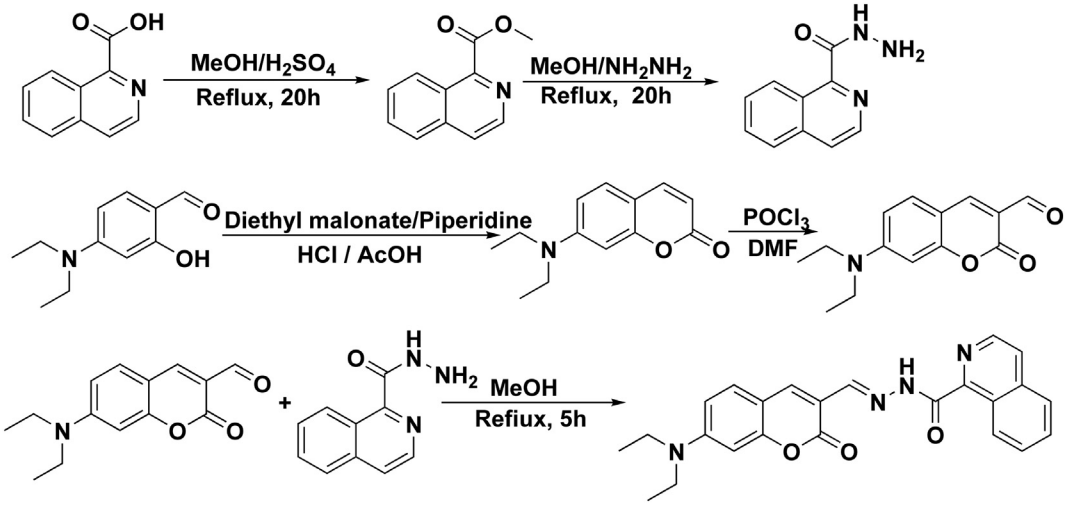

Scheme 1. Syntheses of probe DMI.

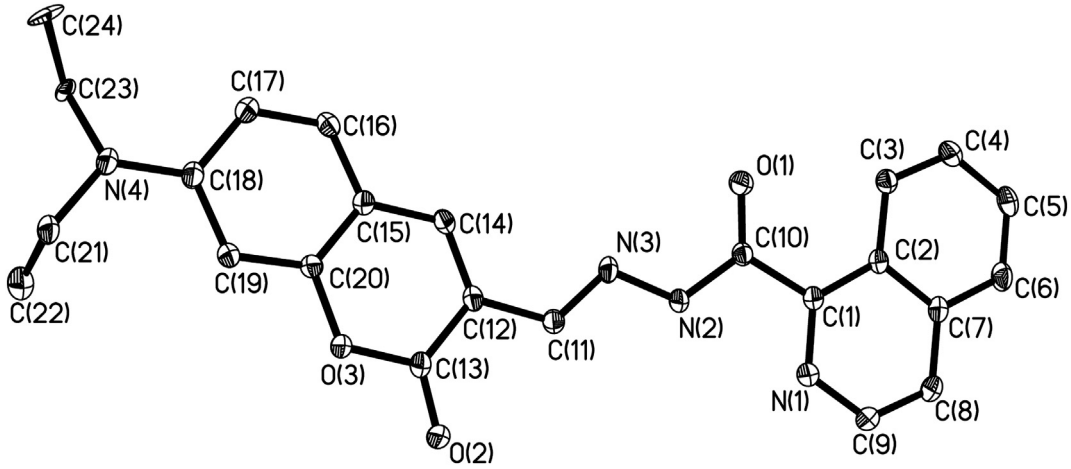

Fig. 1. ORTEP view of DMI molecular structure showing the crystallographic numbering scheme. Thermal ellipsoids are drawn at 30% probability level and all hydrogens are omitted for clarity.

2.5. Cell culture and cytotoxicity studies

MCF-7 cell line was obtained from the American Type Culture Collection (ATCC). MCF-7 cells were kept in growth medias at an atmosphere of 5% CO_2. DMEM (Dulbecco's Modified Eagle Medium) was employed to incubate cells.

The cells were collected and seeded in a 96-well culture plate with a density of 3000 cells each well. The cells were cultivated in a humidified condition containing 5% CO_2 at 37 °C for 24 h. Then, DMI and DMI-Cu^{2+} with different concentrations (100, 50, 25, 12.5, 6.25, 3.125, 1.5625, 0.78125, 0.390625 μM) were added into microplate and fostered for 6 h, respectively. Subsequently, the cells in each well were treated with MTT (10 μL, prepared in DMSO) at a concentration of 5 mg/mL. After another 4 h, excessive MTT solution was removed. 100 μL DMSO was added and OD values were recorded on Infinite 200-Pro Nano Quant Microplate Reader at 570 nm. The cell viabilities were calculated based on following formula: Cell viability (%) = $(OD_{drug} - OD_{blank}) / (OD_{control} - OD_{blank}) \times 100\%$.

2.6. Biological imaging

MCF-7 cells were collected and reseeded in culture plates at 37 °C for 12 h. The cells were separated into three groups. For the first group, DMI (10 μM) were added into the plate and the cells were cultured for 30 min. For the second group, the cells were treated with 10 μM DMI and one equivalent of Cu^{2+} for 30 min successively. For the third group, after being incubated with DMI and Cu^{2+}, S^{2-} (10 μM) was added into the system, which were fostered for another 30 min. The cells were washed three times with PBS and the cell imaging was recorded on confocal laser scanning microscope.

Zebrafish larvae were cultured three days and washed with deionized water before use. Then they were incubated with DMI solution (10 μM, 1 h), DMI (10 μM, 1 h) + Cu^{2+} (10 μM, 1 h) as well as DMI (10 μM, 1 h) + Cu^{2+} (10 μM, 1 h) + S^{2-} (10 μM, 1 h) at room temperature, respectively. After washing zebrafish with deionized water for three times, DMI, Cu^{2+} and S^{2-} were removed and the fluorescent images of zebrafish were observed with an Olympus FV1000 confocal microscope.

3. Results and discussion

3.1. Selectivity of DMI to Cu^{2+}

To evaluate the selectivity of DMI towards Cu^{2+}, UV–vis absorption spectrum of DMI with various metal ions were investigated in CH_3OH-PBS (2 mL, v/v = 3:7) buffer solution. As shown in Fig. S5, a strong

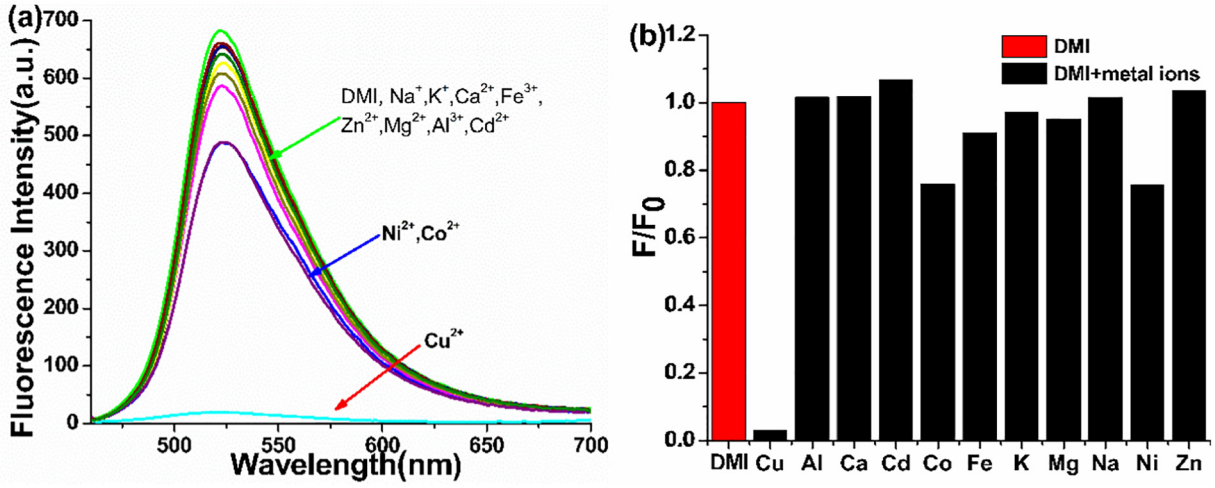

Fig. 2. Fluorescence emission spectra (a) and histogram (b) of probe DMI (10 μM) with addition of various metal ions (10 μM) in CH_3OH-PBS (2 mL, v/v = 3:7) mixed solution.

absorption peak at about 455 nm could be observed, which was the characteristic peak of free probe DMI. Upon addition of various metal ions, Ni^{2+}, Cu^{2+} and Co^{2+} resulted in a reduction of absorbance. The maximum peak in the presence of Cu^{2+} and Co^{2+} exhibited a slight red-shift, while the absorption intensity of Cu^{2+} was higher than that of Co^{2+}. Furthermore, fluorescence selectivity experiment of DMI in the presence of various metal ions was measured in the same system at 450 nm excitation wavelength (Fig. 2). When the metal ions were added into the DMI solution, a slight reduction in fluorescence intensity induced by Ni^{2+}/Co^{2+} and negligible changes induced by other metal ions were observed, which had little influence on the detection of Cu^{2+}. More importantly, the fluorescence response of DMI was quenched distinctly in the presence of Cu^{2+}, which was closely related to the paramagnetic quenching effect of Cu^{2+}. The fluorescence intensity of probe DMI was quenched about 27.4 times by Cu^{2+}. Accordingly, the probe DMI could sense Cu^{2+} with excellent selectivity. Fluorescence intensity of probe DMI and its Cu complex in different proportions of CH_3OH and PBS was measured to select the optimal experimental conditions. As shown in Fig. S6, the fluorescence signal of DMI-Cu^{2+} were quenched in the pure PBS, meanwhile the fluorescence emission of DMI is not very strong. With the increasing proportion of CH_3OH, the fluorescence response of probe DMI was continuously enhanced. Correspondingly, when the ratio of CH_3OH was in the range of 0.4–1, the quenching effect of Cu^{2+} to probe DMI was not obvious. Therefore, in order to ensure the strong fluorescence emission of probe DMI and the good quenching effect of Cu^{2+}, CH_3OH-PBS (v/v = 3:7) phosphate buffer system was selected for the research.

3.2. Sensitivity of DMI to Cu^{2+}

Then, the sensitivity of probe DMI for Cu^{2+} were examined by the UV–vis and fluorescence titrations experiments in CH_3OH-PBS (2 mL, v/v = 3:7) mixed solvent system (10 μM). As shown in Fig. 3a, the representative absorption peak of free probe DMI centered at 455 nm. Upon titration of Cu^{2+} (0–15 μM), the absorption peak at 455 nm was significantly decreased with the appearance of a new absorption peaks at around 525 nm. The formation of well-defined isosbestic points at 270 nm, 335 nm, 385 nm and 492 nm demonstrated that only one combination mode happened between DMI and Cu^{2+}. Furthermore, Fig. 3b illustrated the change of the fluorescence response of probe DMI upon an increasing concentration of Cu^{2+} (0–15 μM). The fluorescence signal of DMI was quenched gradually with addition of Cu^{2+}. All these phenomena indicated the formation of a new complex between DMI and Cu^{2+}.

Based on the fluorescence titration experiments (Fig. 3b inset), we observed that the fluorescence intensity of DMI and Cu^{2+} concentration displayed an excellent linear correlation over the range of 0–10 μM. The limit of detection (LOD) was calculated as 1.52×10^{-8} M by using the following equation: $LOD = K \times Sb1 / S$ ($K = 3$, $Sb1$ was standard deviation of blank solution, S was the slope of linear regression equation) [60,61]. Moreover, the association constant (K) of probe molecule DMI towards Cu^{2+} was estimated to be 2.86×10^4 M^{-1} according to Benesi-Hildebrand plot (Fig. S7) by using following equation:

$$\frac{F_{max} - F_{min}}{F - F_{min}} = \frac{1}{K[M]} + 1$$

where $[M] = Cu^{2+}$, F_{max} and F_{min} were the fluorescence intensity of free probe DMI and in the presence of saturated Cu^{2+}, respectively. F was the fluorescence intensity of Cu complex, which is associated with the concentration of Cu^{2+}.

3.3. Binding mode studies of probe DMI towards Cu^{2+}

To obtain a better insight into the binding mechanism of DMI with Cu^{2+}, Job's plot was explored from the UV–vis absorption data (Fig. S8). When the value of [DMI]/([Cu^{2+}] + [DMI]) was close to 0.66, the UV–vis absorbance displayed an inflection point, which demonstrated the 2:1 stoichiometric binding mode of complex DMI-Cu^{2+}. Furthermore, the mass spectra of complex DMI-Cu^{2+} supported the above result. As shown in Fig. S9, an intense peak for complex DMI-Cu^{2+} was shown at m/z 890.25970, corresponding to the [Cu + 2DMI-H]$^+$, calcd. m/z 890.25961. Thereafter, FT-IR data of DMI (Fig. S4) and its complex DMI-Cu^{2+} (Fig. S10) also confirmed binding mechanism. Compared with the FT-IR spectra of DMI in the absence and presence of Cu^{2+}, the C═O peak of DMI at 1678.21 cm^{-1}, C═N peak at 1617.78 cm^{-1} were shifted to 1605.16 cm^{-1} (C═O) and 1573.93 cm^{-1} (C═N) with the weakness of the corresponding bands, respectively, which confirmed that the functional groups C═O and C═N of probe DMI participated in the interaction with Cu^{2+}.

3.4. Density functional theoretical calculations

In order to further clarify the electronic properties, the geometry optimisations of DMI and its complex DMI-Cu^{2+} were performed on the Gaussian 09 program at DFT/B3LYP level. As shown in Fig. S11, the

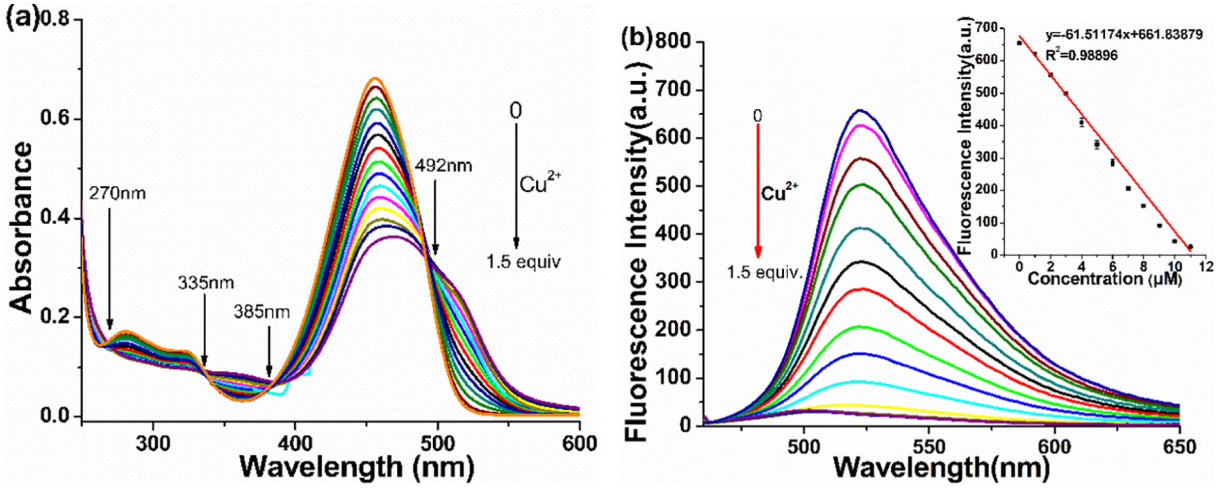

Fig. 3. UV–vis (a) and fluorescence (b) titration spectra of probe DMI (10 μM) with addition of different Cu^{2+} concentrations (0–15 μM) in CH_3OH-PBS (2 mL, v/v = 3:7) mixed solution. λ_{ex} = 450 nm. Inset: the linear relationship between the fluorescence intensity at 521 nm and the Cu^{2+} concentration (Error bars, SD, n = 3).

probe DMI possessed good planarity with an extended conjugation, containing coumarin ring, iso-quinoline ring and hydrazine group. In the DMI system, the dihedral angles between coumarin ring and hydrazide group, coumarin ring and iso-quinoline ring as well as iso-quinoline ring and hydrazide group were 0.352°, 0.162° and 0.194°, respectively, which were highly close to the crystal structure of DMI. The interaction between probe DMI and Cu^{2+} destroyed the planarity of the whole molecular and three dihedral angles mentioned above twisted to 12.4222°, 35.788° and 47.683°, respectively. The HOMO and LUMO orbital energy levels of probe DMI and its complex DMI-Cu^{2+} were shown in Fig. 4. The HOMO-LUMO energy gap of probe DMI and Cu complex were 3.118 eV and 2.725 eV, respectively, which were in agreement with the generation of red shifted absorption band upon incrementally addition of Cu^{2+} to DMI.

3.5. The probe DMI-Cu^{2+} for detection of S^{2-}

Based on the strong binding affinity of Cu^{2+} to S^{2-}, we supposed that the complex DMI-Cu^{2+} could act as a probe for the detection of S^{2-}. Therefore, the selectivity of DMI-Cu^{2+} towards S^{2-} was studied. The influence of different tested analytes, including S^{2-}, Br^-, CH_3COO^-, Cl^-, Cys, F^-, $H_2PO_4^-$, HPO_4^{2-}, HSO_3^-, NO_2^-, NO_3^- and GSH were measured. As shown in Fig. 5, except a minor fluorescence enhancement upon addition of Cys and GSH, which is caused by the strong binding affinity of Cu^{2+} towards sulfur-containing molecules, only S^{2-} induced a significant change of 10.67-folds fluorescence increase. Meanwhile, competitive experiment (Fig. S12) showed there were no obvious changes induced by coexistent ions and biothiol, indicating

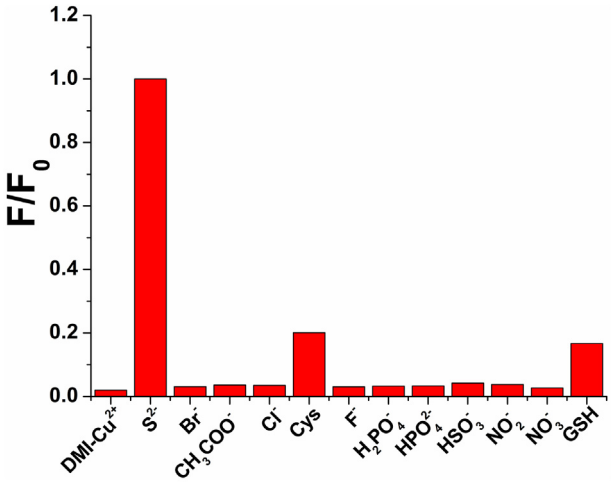

Fig. 5. Fluorescence response of DMI-Cu^{2+} (10 μM) in the presence of different tested analytes (10 μM) in CH_3OH-PBS (2 mL, v/v = 3:7) mixed solution.

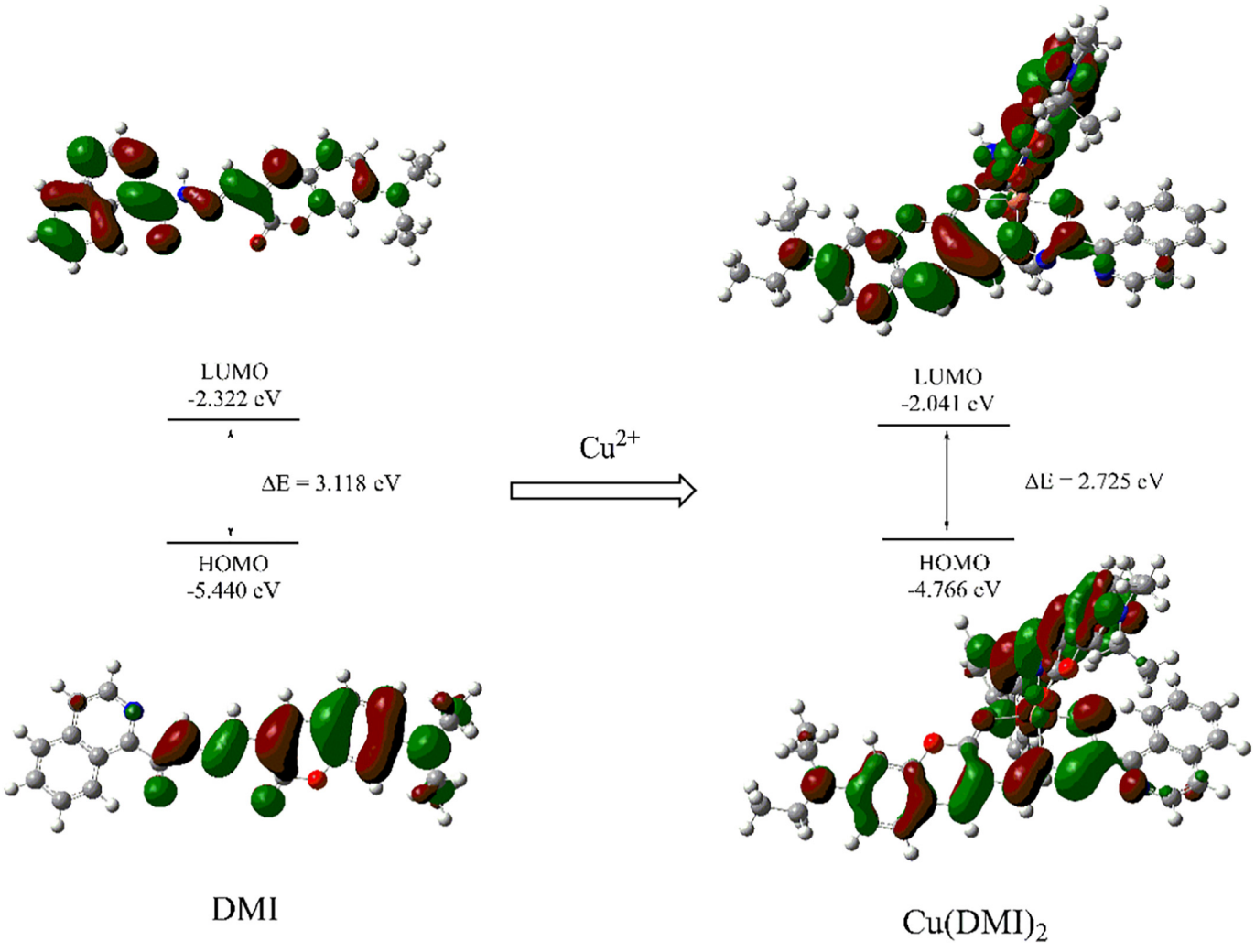

Fig. 4. Frontier molecular orbitals of probe DMI and its complex DMI-Cu^{2+}.

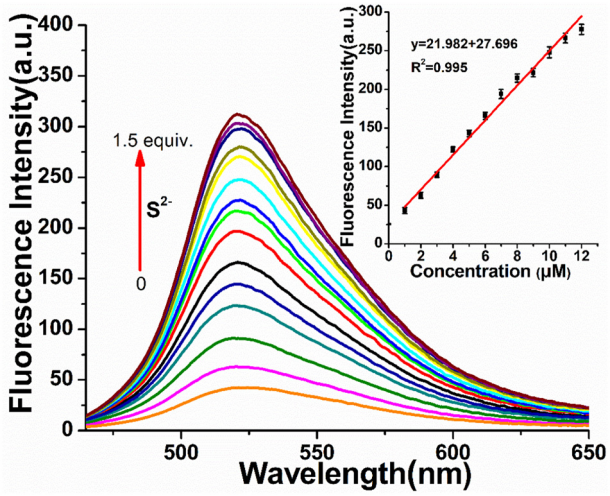

Fig. 6. Fluorescence titration spectra of probe DMI-Cu^{2+} (10 μM) with addition of different S^{2-} concentrations (0–15 μM) in CH_3OH-PBS (2 mL, v/v = 3:7) mixed solution. λ_{ex} = 450 nm. Inset: the linear relationship between the fluorescence intensity at 521 nm and the S^{2-} concentration (Error bars, SD, $n = 3$).

the complex DMI-Cu^{2+} possessed a predominant selectivity to S^{2-}. Furthermore, fluorescence titration experiment of DMI-Cu^{2+} to S^{2-} was investigated. As shown in Fig. 6, upon increasing S^{2-} concentrations, the fluorescence responses were gradually enhanced. From Fig. 6 inset, good linearity between the fluorescence intensity and S^{2-} concentration was obtained in the range of 0–14 μM. The limit of detection to S^{2-} was 1.79×10^{-8} M (Fig. S13), which was lower than the maximum allowable level set by WHO (15 μM). These results indicated that the complex DMI-Cu^{2+} could be employed as a probe to detect S^{2-} directly with high selectivity and sensitivity.

3.6. Effect of pH

The good sensing performance of probe in suitable pH range played a vital role in practical applications. Therefore, the effects of pH (2–11) on fluorescence response of probe DMI and its complex DMI-Cu^{2+} were further measured in CH_3OH-PBS (2 mL, v/v = 3:7) mixed solution (Fig. S14). For free probe DMI, the fluorescence intensity increased and reached to maximum at about pH 7. At the same time, the intensity of DMI-Cu^{2+} decreased and reached to minimum within the same pH level. These phenomena confirmed that DMI and its complex DMI-Cu^{2+} possessed the best fluorescence performance at physiological pH range (7–8) and could act as practical probes to detect Cu^{2+} and S^{2-} in living organisms.

3.7. Bioimaging application

3.7.1. Cytotoxicity and cell imaging

Encouraged by the high selectivity and sensitivity of DMI towards Cu^{2+} as well as DMI-Cu^{2+} towards S^{2-} in physiological pH range, DMI and DMI-Cu^{2+} were utilized to study potential applications on fluorescent bio-imaging in living MCF-7 cells [62]. Initially, the cytotoxicity of DMI and DMI-Cu^{2+} was evaluated by MTT method with different concentrations. Although the MCF-7 cells were treated by DMI and DMI-Cu^{2+} even at higher concentration (25 μM), the survival degrees were more than 95% (Fig. 7a) and 80% (Fig. 7b), respectively, indicating DMI and DMI-Cu^{2+} could act as bioprobes and were suitable for intracellular detection.

Then, owing to the low cytotoxicity of DMI and DMI-Cu^{2+}, the fluorescent imaging was captured in MCF-7 cell line (Fig. 8). When the cells were fostered with DMI (10 μM) for 30 min at room temperature, a very strong green fluorescence signal was observed. Nevertheless, the fluorescence signal was quenched upon incubation with Cu^{2+} (10 μM) for another 30 min, which was ascribed to the combination of DMI and Cu^{2+}. Further treatment with S^{2-} under the same experiment condition made the fluorescence response recover. These observations indicated that DMI was capable of penetrating cell membranes and could be served as a probe to sense Cu^{2+} and S^{2-} visually in living cells.

3.7.2. Zebrafish imaging

Comparing with the excellent properties of cell imaging, monitoring Cu^{2+}/S^{2-} in living animals was more significant and meaningful. As an advanced creature, zebrafish had the advantages of optical transparency, simple operation and genetic similarities to human beings [63]. Herein, fluorescence imaging of zebrafish was further investigated by using confocal microscope FV1000 (Fig. 9). Incubating zebrafish with DMI (10 μM) merely for 1 h, brightly green fluorescence signal was collected in head and digestive system. Then treated zebrafish with Cu^{2+} (10 μM), the green fluorescence response diminished significantly. After 1 h, one equivalent of S^{2-} was added and the strong green fluorescence signal was restored. These phenomena signified that DMI and DMI-Cu^{2+} could potentially apply in biological system to monitor Cu^{2+} and S^{2-}, respectively.

3.8. Actual sample testing

Since S^{2-} is one of the most common anions in our life, detecting S^{2-} is of great importance. When the blood was rotten, many substances

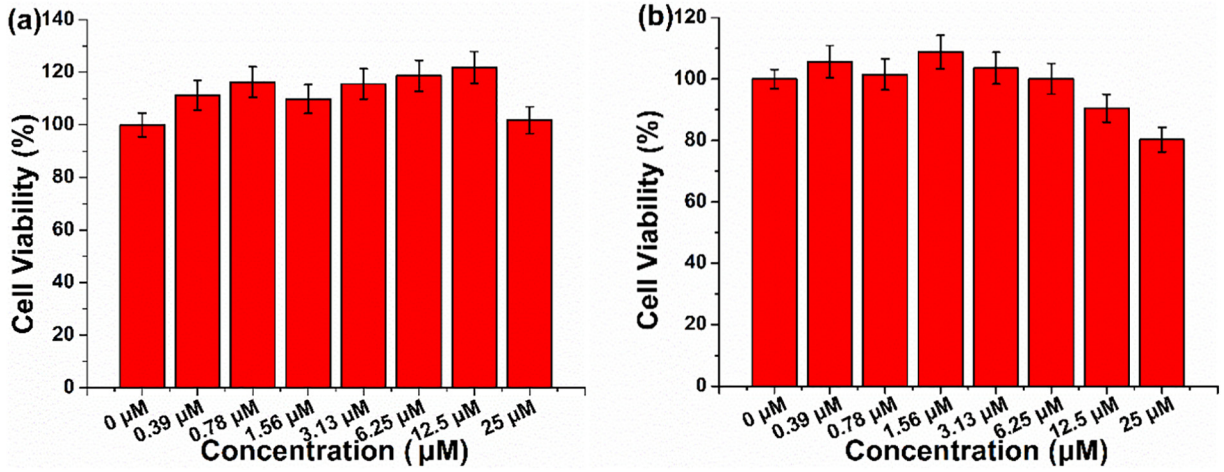

Fig. 7. Cell viability of MCF-7 cells incubated by different concentration (0.39–25 μM) of DMI (a) and DMI-Cu^{2+} (b) for 6 h at room temperature.

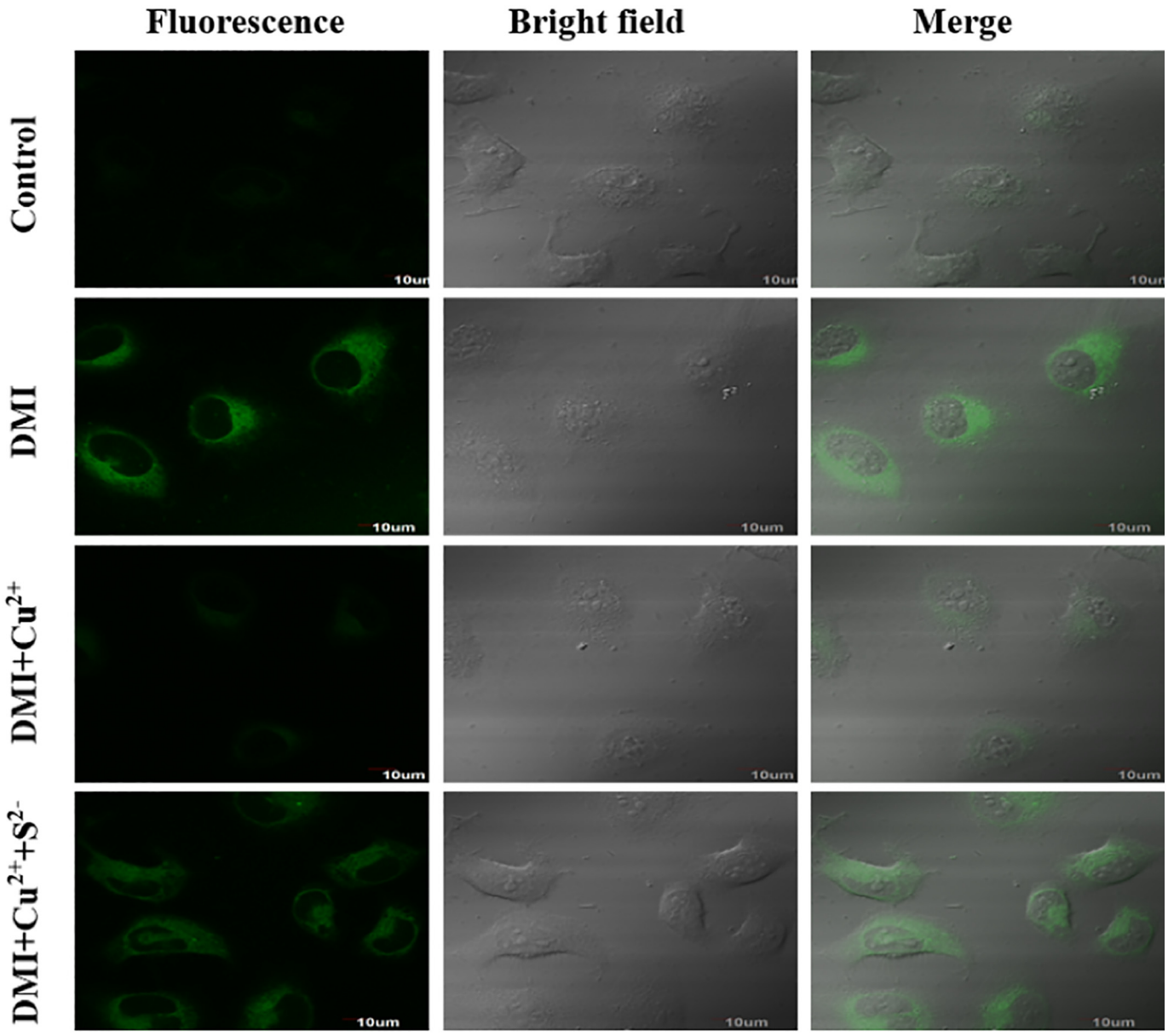

Fig. 8. Confocal fluorescence imaging of living cells incubated with DMI (10 μM) for 1 h, and then incubated with Cu^{2+} (10 μM) and S^{2-} (10 μM) successively for another 1 h. Bright field image (left), fluorescence image (middle), superposition image (right). $\lambda_{ex} = 405$ nm.

including hydrogen sulfide, mercaptan, sulfide, ammonia, methane, carbon dioxide were produced. According to the above experiments, the probe DMI- Cu^{2+} was utilized to detect S^{2-} induced by blood corruption. Corrupt blood samples at different times (including 0, 2, 4, 6, 8, 12, 24 h) were prepared and added into DMI-Cu^{2+} solution (10 μM). Then, the fluorescence intensity of system was measured. As shown in Fig. S15, the fluorescence intensity increased with the time of blood corruption, indicating more hydrogen sulfide was produced. This result demonstrated that the probe DMI-Cu^{2+} could be applied to detect actual sulfur samples preliminarily and calculate time of death.

4. Conclusion

In summary, a novel fluorescence probe DMI was described in this paper, which had been successfully developed, synthesized and characterized. The green emitting fluorescence of probe DMI could be quenched by Cu^{2+}, and the fluorescence response recovered with the addition of S^{2-} subsequently. The probe DMI and DMI-Cu^{2+} showed excellent fluorescence properties of high selectivity and sensitivity towards Cu^{2+}/S^{2-} at pH 7 in CH_3OH-PBS (v/v = 3:7) mixed solution. Various experiments, including Job's plot, ESI-MS, IR spectrometry and DFT calculations, confirmed the binding mode of DMI to Cu^{2+}. Its application in cell and zebrafish imaging indicated that the probe had the ability to monitor Cu^{2+} and S^{2-} in living cells and biological system. The detection of S^{2-} using DMI-Cu^{2+} in corrupt blood samples could estimate the death time.

CRediT authorship contribution statement

Xiao-Jing Yan: Conceptualization, Methodology, Investigation, Writing - original draft.**Zhi-Gang Wang:**Data curation, Software, Visualization.**Yang Wang:**Investigation, Validation, Formal analysis.**Yu-Ying Huang:**Investigation, Resources.**Hai-Bo Liu:**Software, Resources, Writing - review & editing, Funding acquisition.**Cheng-Zhi Xie:**Methodology, Writing - original draft, Supervision, Funding acquisition.**Qing-**

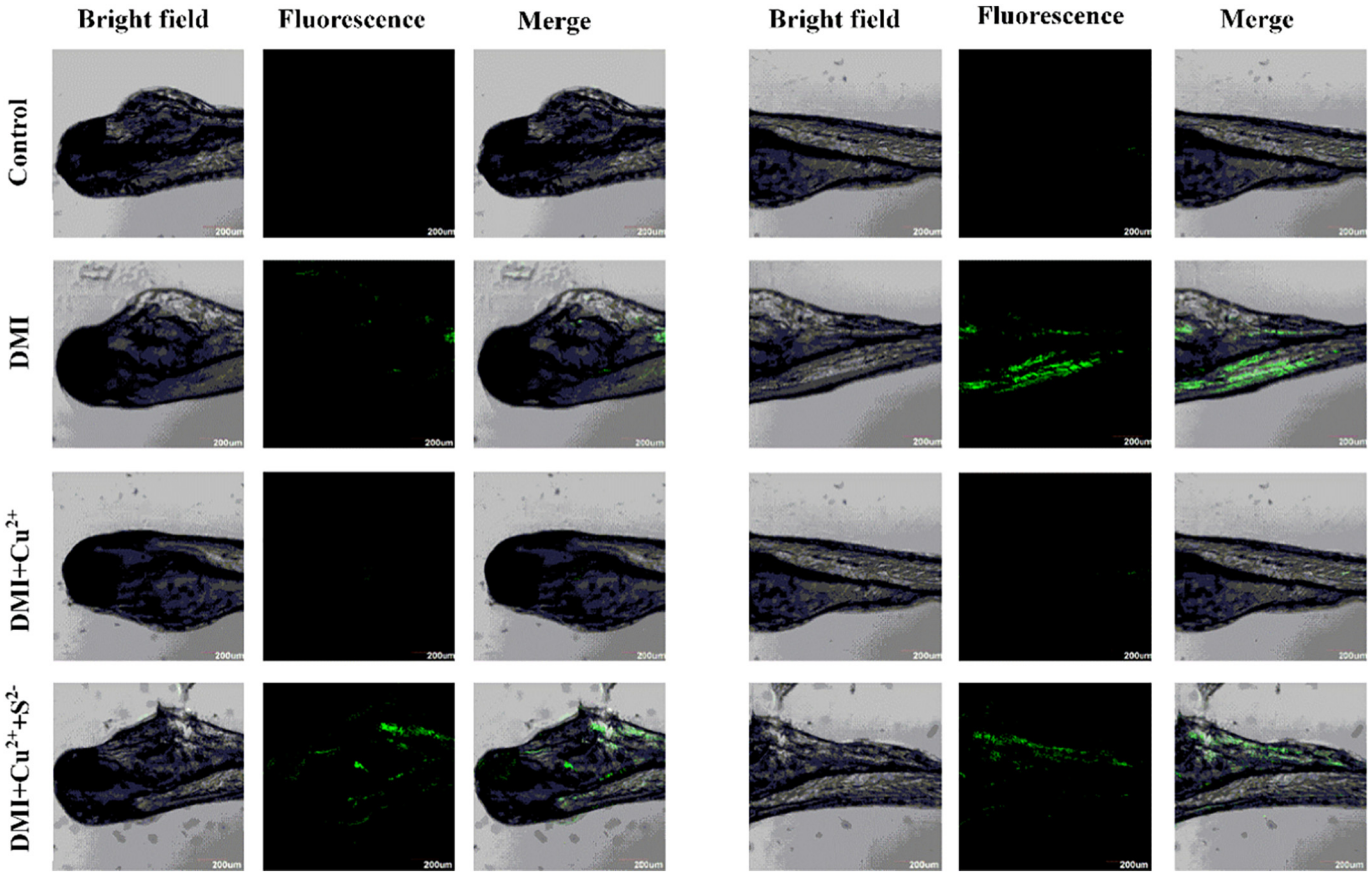

Fig. 9. Confocal fluorescence imaging of zebrafish incubated with DMI (10 μM) for 1 h, and then incubated with Cu^{2+} (10 μM) and S^{2-} (10 μM) successively for another 1 h. Bright field image (left), fluorescence image (middle), superposition image (right). $\lambda_{ex} = 405$ nm.

Zhong Li: Software.**Jing-Yuan Xu:**Conceptualization, Supervision, Project administration, Funding acquisition.

Declaration of competing interest

The authors declare that they have no known competing financial interests or personal relationships that could have appeared to influence the work reported in this paper.

Acknowledgments

This work was supported by National Natural Science Foundation of China (No. 21977080), Tianjin Natural Science Foundation (No. 17JCZDJC33100, 18JCYBJC91300) and CAMS Innovation Fund for Medical Sciences (CIFMS) (2016-I2M-3-015).

Appendix A. Supplementary data

Supplementary data to this article can be found online at https://doi.org/10.1016/j.saa.2020.118797.

References

[1] X.L. Xie, X.P. Chen, B. Li, L.M. Zhang, Study on a highly selective colorimetric chemosensor for Cu^{2+} detection and its indirect sensing for hypochlorite, Dyes Pigments 98 (2013) 422–427, https://doi.org/10.1016/j.dyepig.2013.03.022.

[2] G. Sivaraman, M. Iniya, T. Anand, N.G. Kotla, O. Sunnapu, S. Singaravadivel, A. Gulyani, D. Chellappa, Chemically diverse small molecule fluorescent chemosensors for copper ion, Coord. Chem. Rev. 357 (2018) 50–104, https://doi.org/10.1016/j.ccr.2017.11.020.

[3] G.G.V. Kumar, M.P. Kesavan, G. Sivaraman, J. Annaraj, K. Anitha, A. Tamilselvi, S. Athimoolam, B. Sridhar, J. Rajesh, Reversible NIR fluorescent probes for Cu^{2+} ions detection and its living cell imaging, Sensors Actuators B Chem. 255 (2018) 3235–3247, https://doi.org/10.1016/j.snb.2017.09.150.

[4] Y.X. Li, H.P. Zhou, S.H. Yin, H. Jiang, N. Niu, H. Huang, S.A. Shahzad, C. Yu, A BOPHY probe for the fluorescence turn-on detection of Cu^{2+}, Sensors Actuators B Chem. 235 (2016) 33–38, https://doi.org/10.1016/j.snb.2016.05.055.

[5] R.A. Løvstad, A kinetic study on the distribution of Cu(II)-ions between albumin and transferrin, Biometals 17 (2004) 111–113, https://doi.org/10.1023/B:BIOM.0000018362.37471.0b.

[6] Q.T. Meng, R. Zhang, H.M. Jia, X. Gao, C.P. Wang, Y. Shi, Z.Q. Zhang, A reversible fluorescence chemosensor for sequentially quantitative monitoring copper and sulfide in living cells, Talanta 143 (2015) 294–301, https://doi.org/10.1016/j.talanta.2015.04.072.

[7] S.J. Ranee, G. Sivaraman, A.M. Pushpalatha, S Muthusubramanian, Quinoline based sensors for bivalent copper ions in living cells, Sensors Actuators B Chem. 255 (2018) 630–637, https://doi.org/10.1016/j.snb.2017.08.111.

[8] K.Y. Ryu, J. Lee, J.A. Kim, D.Y. Park, C. Kim, Colorimetric chemosensor for multiple targets, Cu^{2+}, CN^{-} and S^{2-}, RSC Adv. 6 (2016) 16586–16597, https://doi.org/10.1039/C5RA27553A.

[9] S. Ayton, P. Lei, A.I. Bush, Metallostasis in Alzheimer's disease, Free Radic. Biol. Med. 62 (2013) 76–89, https://doi.org/10.1016/j.freeradbiomed.2012.10.558.

[10] K.J. Barnham, C.L. Masters, A.I. Bush, Neurodegenerative diseases and oxidative stress, Nat. Rev. Drug Discov. 3 (2004) 205–214, https://doi.org/10.1038/nrd1330.

[11] O.M. Siggs, J.T. Cruite, X. Du, S. Rutschmann, E. Masliah, B. Beutler, M.B.A. Oldstone, Disruption of copper homeostasis due to a mutation of Atp7a delays the onset of prion disease, Proc. Natl. Acad. Sci. 109 (2012) 13733–13738, https://doi.org/10.1073/pnas.1211499109.

[12] D.T. Quang, J.S. Kim, Fluoro- and chromogenic chemodosimeters for heavy metal ion detection in solution and biospecimens, Chem. Rev. 110 (2010) 6280–6301, https://doi.org/10.1073/10.1021/cr100154p.

[13] Y.L. Pak, J. Li, K.C. Ko, G. Kim, J.Y. Lee, J. Yoon, Mitochondria-targeted reaction-based fluorescent probe for hydrogen sulfide, Anal. Chem. 88 (2016) 5476–5481, https://doi.org/10.1021/acs.analchem.6b00956.

[14] T. Fang, X.D. Jiang, C. Sun, Q. Li, BODIPY-based naked-eye fluorescent on-off probe with high selectivity for H_2S based on thiolysis of dinitrophenyl ether, Sensors Actuators B Chem. 290 (2019) 551–557, https://doi.org/10.1016/j.snb.2019.03.141.

[15] S. Yang, Y. Qi, C.H. Liu, Y.J. Wang, Y.R. Zhao, L.L. Wang, J.S. Li, W.H. Tan, R.H. Yang, Design of a simultaneous target and location-activatable fluorescent probe for

visualizing hydrogen sulfide in lysosomes, Anal. Chem. 15 (2014) 7508–7515, https://doi.org/10.1021/ac501263d.
[16] X.R. Shi, C.X. Yin, Y. Wen, F.J. Huo, A dual-sites fluorescent probe based on symmetric structure of naphthalimide derivative to detect H_2S, Dyes Pigments 165 (2019) 38–43, https://doi.org/10.1016/j.dyepig.2019.02.014.
[17] K. Yao, D. Caruntu, M. Zeng, J. Chen, C. O'Connor, W. Zhou, Parts per billion-level H_2S detection at room temperature based on self-assembled In_2O_3 nanoparticles, J. Phys. Chem. C 113 (2009) 14812–14817, https://doi.org/10.1021/jp905189f.
[18] P. Mateus, R. Delgado, V. Andre, D.M. Teresa, Sulfate recognition by a hexaaza cryptand receptor, Org. Biomol. Chem. 13 (2015) 834–842, https://doi.org/10.1039/C4OB02027H.
[19] M.M. Yu, W.W. Du, W. Zhou, H.X. Li, C.X. Liu, L.H. Wei, Z.X. Li, H.Y. Zhang, A 1,8-naphthalimide-based chemosensor with an off-on fluorescence and lifetime imaging response for intracellular Cr^{3+} and further for S^{2-}, Dyes Pigments 126 (2016) 279–285, https://doi.org/10.1016/j.dyepig.2015.12.001.
[20] Y. Cai, L. Li, Z. Wang, J.Z. Sun, A. Qin, B.Z. Tang, A sensitivity tuneable tetraphenylethene-based fluorescent probe for directly indicating the concentration of hydrogen sulfide, Chem. Commun. 50 (2014) 8892–8895, https://doi.org/10.1039/C4CC02844A.
[21] L.F. Hu, M. Lu, C.X. Tiong, G.S. Dawe, G. Hu, J.S. Bian, Neuroprotective effects of hydrogen sulfide on Parkinson's disease rat models, Aging Cell 9 (2010) 135–146, https://doi.org/10.1111/j.1474-9726.2009.00543.x.
[22] D. Giuliani, A. Ottani, D. Zaffe, M. Galantucci, F. Strinati, R. Lodi, S. Guarini, Hydrogen sulfide slows down progression of experimental Alzheimer's disease by targeting multiple pathophysiological mechanisms, Neurobiol. Learn. Mem. 104 (2013) 82–91, https://doi.org/10.1016/j.nlm.2013.05.006.
[23] C.R. Liu, B. Peng, S. Li, C.M. Park, A.R. Whorton, M. Xian, Reaction based fluorescent probes for hydrogen sulfide, Org. Lett. 14 (2012) 2184–2187, https://doi.org/10.1021/ol3008183.
[24] S. Fiorucci, E. Distrutti, G. Cirino, J.L. Wallace, The emerging roles of hydrogen sulfide in the gastrointestinal tract and liver, Gastroenterology 131 (2006) 259–271, https://doi.org/10.1053/j.gastro.2006.02.033.
[25] O. Kabil, R. Banerjee, Redox biochemistry of hydrogen sulfide, J. Biol. Chem. 285 (2010) 21903–21907, https://doi.org/10.1074/jbc.R110.128363.
[26] Y. Qian, J. Lin, T.B. Liu, H.L. Zhu, Living cells imaging for copper and hydrogen sulfide by a selective "on-off-on" fluorescent probe, Talanta 132 (2015) 727–732, https://doi.org/10.1016/j.talanta.2014.10.034.
[27] Y.F. Zhu, D.H. Fan, W.Z. Shen, A general chemical conversion route to synthesize various ZnO-based core/shell structures, J. Phys. Chem. C 112 (2008) 10402–10406, https://doi.org/10.1021/jp802545e.
[28] L.W. He, W.Y. Lin, Q.Y. Xu, H.P. Wei, A new strategy to construct a FRET platform for ratiometric sensing of hydrogen sulfide, Chem. Commun. 8 (2015) 1510–1513, https://doi.org/10.1039/c4cc08522a.
[29] X. Zhou, S. Lee, Z. Xu, J. Yoon, Recent progress on the development of chemosensors for gases, Chem. Rev. 115 (2015) 7944–8000, https://doi.org/10.1021/cr500567r.
[30] L.A. Montoya, M.D. Pluth, Hydrogen sulfide deactivates common nitrobenzofurazan-based fluorescent thiol labeling reagents, Anal. Chem. 12 (2014) 6032–6039, https://doi.org/10.1021/ac501193r.
[31] M.Q. Wang, K. Li, J.T. Hou, BINOL-based fluorescent sensor for recognition of Cu(II) and sulfide anion in water, J. Organomet. Chem. 77 (2012) 8350–8354, https://doi.org/10.1021/jo301196m.
[32] J. Huang, M. Tang, M. Liu, M. Zhou, Z. Liu, Y. Cao, M. Zhu, S. Liu, W. Zeng, Development of a fast responsive and highly sensitive fluorescent probe for Cu^{2+} ion and imaging in living cells, Dyes Pigments 107 (2014) 1–8, https://doi.org/10.1016/j.dyepig.2014.02.022.
[33] H.J. Jang, T.G. Jo, C. Kim, A single colorimetric sensor for multiple targets: the sequential detection of Co^{2+} and cyanide and the selective detection of Cu^{2+} in aqueous solution, RSC Adv. 7 (2017) 17650–17659, https://doi.org/10.1039/C7RA01580A.
[34] Y.S. Hu, J. Kang, P.P. Zhou, X. Han, J.Y. Sun, S.D. Liu, L.W. Zhang, J.G. Fang, A selective colorimetric and red-emitting fluorometric probe for sequential detection of Cu^{2+} and H_2S, Sensors Actuators B Chem. 255 (2018) 3155–3162, https://doi.org/10.1016/j.snb.2017.09.140.
[35] Y. Liu, Y. Duan, A.D. Gill, L. Perez, Q. Jiang, R.J. Hooley, W. Zhong, Metal-assisted selective recognition of biothiols by a synthetic receptor array, Chem. Commun. 54 (2018) 13147–13150, https://doi.org/10.1039/c8cc07220e.
[36] Z.Q. Hu, L.L. Sun, Y.Y. Gu, Y. Jiang, A sensitive and selective fluorescent probe for detection of glutathione in the presence of Cu^{2+} and its application to biological imaging, Sensors Actuators B Chem. 212 (2015) 220–224, https://doi.org/10.1016/j.snb.2015.01.084.
[37] P. Wang, J. Wu, C. Di, R. Zhou, H. Zhang, A novel peptide-based fluorescence chemosensor for selective imaging of hydrogen sulfide both in living cells and zebrafish, Biosens. Bioelectron. 92 (2017) 602–609, https://doi.org/10.1016/j.bios.2016.10.050.
[38] X. Wu, H. Li, Y. Kan, B. Yin, A regeneratable and highly selective fluorescent probe for sulfide detection in aqueous solution, Dalton Trans. 42 (2013) 16302–16310, https://doi.org/10.1039/c3dt51953h.
[39] A. Paul, S. Anbu, G. Sharma, M.L. Kuznetsov, M.F.C.G.D. Silva, B. Koch, A.J.L. Pombeiro, Intracellular detection of Cu^{2+} and S^{2-} ions through a quinazoline functionalized benzimidazole-based new fluorogenic differential chemosensor, Dalton Trans. 44 (2015) 16953–16964, https://doi.org/10.1039/C5DT02662H.
[40] F.B. Yu, P. Li, P. Song, An ICT-based strategy to a colorimetric and ratiometric fluorescence probe for hydrogen sulfide in living cells, Chem. Commun. 48 (2012) 2852–2860, https://doi.org/10.1039/C2CC17658K.
[41] S. Palanisamy, L.Y. Lee, Y.L. Wang, Y.J. Chen, C.Y. Chen, Y.M. Wang, A water soluble and fast response fluorescent turn-on copper complex probe for H_2S detection in zebra fish, Talanta 147 (2016) 445–452, https://doi.org/10.1016/j.talanta.2015.10.019.
[42] C.S. Kwan, T. Wang, S.M. Chan, Z.W. Cai, K.C.F. Leung, Selective detection of sulfide in human lung cancer cells with a blue-fluorescent "ON-OFF-ON" benzimidazole-based chemosensor ensemble, Dalton Trans. 17 (2020) 5445–5453, https://doi.org/10.1039/d0dt00031K.
[43] P. Sakthive, K. Sekar, G. Sivaraman, S. Singaravadivel, Rhodamine–benzothiazole conjugate as an efficient multimodal sensor for Hg^{2+} ions and its application to imaging in living cells, New J. Chem. 42 (2018) 11665–11672, https://doi.org/10.1039/C8NJ01736K.
[44] S.Y. Wu, Y.N. Lin, J.W. Liu, W. Shi, G.M. Yang, P. Cheng, Rapid detection of the biomarkers for carcinoid tumors by a water stable luminescent lanthanide metal-organic framework, Adv. Funct. Mater. 28 (2018) 1707169, https://doi.org/10.1002/adfm.201707169.
[45] S.Y. Zhang, W. Shi, P. Cheng, M.J. Zaworotko, A mixed-crystal lanthanide zeolite-like metal-organic framework as a fluorescent indicator for lysophosphatidic acid, a cancer biomarker, J. Am. Chem. Soc. 137 (2015) 12203–12206, https://doi.org/10.1021/jacs.5b06929.
[46] F. Yan, Y. Yang, Y.Z. Wang, Dual-functional colorimetric fluorescent probe for sequential Cu^{2+} and S^{2-} detection in bio-imaging, Sensors Actuators B Chem. 288 (2019) 27–37, https://doi.org/10.1016/j.snb.2019.02.062.
[47] Y. Jiao, L. Zhou, H.Y. He, J.Q. Yin, C.Y. Duan, A new fluorescent chemosensor for recognition of Hg^{2+} ions based on a coumarin derivative, Talanta 162 (2017) 403–407, https://doi.org/10.1016/j.talanta.2016.10.004.
[48] K.P. Wang, Y. Lei, J.P. Chen, Z.H. Ge, W. Liu, Q. Zhang, S.J. Chen, Z.Q. Hu, The coumarin conjugate: synthesis, photophysical properties and the ratiometric fluorescence response to water content of organic solvent, Dyes Pigments 151 (2018) 233–237, https://doi.org/10.1016/j.dyepig.2018.01.004.
[49] H. Zhang, L.Z. Xu, W.Q. Chen, J. Huang, C.S. Huang, J.R. Sheng, X.Z. Song, Simultaneous discrimination of cysteine, homocysteine, glutathione, and H_2S in living cells through a multisignal combination strategy, Anal. Chem. 91 (2019) 1904–1911, https://doi.org/10.1021/acs.analchem.8b03869.
[50] Y. Wang, Z.G. Wang, X.Q. Song, Q. Chen, H. Tian, C.Z. Xie, Q.Z. Li, J.Y. Xu, Dual functional turn-on non-toxic chemosensor for highly selective and sensitive visual detection of Mg^{2+} and Zn^{2+}: solventcontrolled recognition effect and bio-imaging application, Analyst. 144 (2019) 4024–4032, https://doi.org/10.1039/C9AN00583H.
[51] W. Xu, G.J. Han, P.Y. Ma, Q.P. Diao, L.B. Xu, X. Liu, Y. Sun, X.H. Wang, D.Q. Song, A highly selective turn-on fluorescent and chromogenic probe for CN^- and its applications in imaging of living cells and zebrafish in vivo, Sensors Actuators B Chem. 251 (2017) 366–373, https://doi.org/10.1016/j.snb.2017.05.137.
[52] Z.G. Wang, Y. Wang, X.J. Ding, Y.X. Sun, H.B. Liu, C.Z. Xie, J. Qian, Q.Z. Li, J.Y. Xu, A highly selective colorimetric and fluorescent probe for quantitative detection of Cu^{2+}/Co^{2+}: the unique ON-OFF-ON fluorimetric detection strategy and applications in living cells/zebrafish, Spectrochim. Acta A 228 (2020) 117763, https://doi.org/10.1016/j.saa.2019.117763.
[53] Z.G. Wang, X.J. Ding, Y.Y. Huang, X.J. Yan, B. Ding, Q.Z. Li, C.Z. Xie, J.Y. Xu, The development of coumarin Schiff base system applied as highly selective fluorescent/colorimetric probes for Cu^{2+} and tumor biomarker glutathione detection, Dyes Pigments 175 (2020) 108156, https://doi.org/10.1016/j.dyepig.2019.108156.
[54] Y. Wang, Z.Y. Ma, D.L. Zhang, J.L. Deng, X. Chen, C.Z. Xie, X. Qiao, Q.Z. Li, J.Y. Xu, Highly selective and sensitive turn-on fluorescent sensor for detection of Al^{3+} based on quinoline-base Schiff base, Spectrochim. Acta A 195 (2018) 157–164, https://doi.org/10.1016/j.saa.2018.01.049.
[55] N. Mergu, M. Kim, Y.A. Son, A coumarin-derived Cu^{2+}-flluorescent chemosensor and its direct application in aqueous media, Spectrochim. Acta A 188 (2018) 571–580, https://doi.org/10.1016/j.saa.2017.07.047.
[56] M.J. Frisch, G.W. Trucks, H.B. Schlegel, G.E. Scuseria, M.A. Robb, J.R. Cheeseman, G. Scalmani, V. Barone, B. Mennucci, G.A. Petersson, H. Nakatsuji, M. Caricato, X. Li, H.P. Hratchian, A.F. Izmaylov, J. Bloino, G. Zheng, J.L. Sonnenberg, M. Hada, M. Ehara, K. Toyota, R. Fukuda, J. Hasegawa, M. Ishida, T. Nakajima, Y. Honda, O. Kitao, H. Nakai, T. Vreven, J.A. Montgomery Jr., J.E. Peralta, F. Ogliaro, M. Bearpark, J.J. Heyd, E. Brothers, K.N. Kudin, V.N. Staroverov, R. Kobayashi, J. Normand, K. Raghavachari, A. Rendell, J.C. Burant, S.S. Iyengar, J. Tomasi, M. Cossi, N. Rega, J.M. Millam, M. Klene, J.E. Knox, J.B. Cross, V. Bakken, C. Adamo, J. Jaramillo, R. Gomperts, R.E. Stratmann, O. Yazyev, A.J. Austin, R. Cammi, C. Pomelli, J.W. Ochterski, R.L. Martin, K. Morokuma, V.G. Zakrzewski, G.A. Voth, P. Salvador, J.J. Dannenberg, S. Dapprich, A.D. Daniels, O. Farkas, J.B. Foresman, J.V. Ortiz, J. Cioslowski, D.J. Fox, Gaussian, Inc., Wallingford CT, 2009.
[57] C.P.J. Shanmugapriya, S. Singaravadivel, G. Sivaraman, D. Chellappa, Anthracene-based highly selective and sensitive fluorescent "turn-on" chemodosimeter for Hg^{2+}, ACS Omega 3 (2018) 12584–12592, https://doi.org/10.1021/acsomega.8b01142.
[58] G.G.V. Kumar, M.P. Kesavan, A. Tamilselvi, G. Rajagopal, J.D. Raja, K. Sakthipandi, J. Rajesh, G. Sivaraman, A reversible fluorescent chemosensor for the rapid detection of Hg^{2+} in an aqueous solution: its logic gates behavior, Sensors Actuators B Chem. 273 (2018) 305–315, https://doi.org/10.1016/j.snb.2018.06.067.
[59] G. Sivaraman, T. Anand, D. Chellappa, A fluorescence switch for the detection of nitric oxide and histidine and its application in live cell imaging, ChemPlusChem 79 (2014) 1761–1766, https://doi.org/10.1002/cplu.201402217.
[60] G.G.V. Kumar, M.P. Kesavan, G. Sivaraman, J. Rajesh, Colorimetric and NIR fluorescence receptors for F^- ion detection in aqueous condition and its live cell imaging, Sensors Actuators B Chem. 255 (2018) 3194–3206, https://doi.org/10.1016/j.snb.2017.09.145.
[61] G. Sivaraman, B. Vidya, D. Chellappa, Rhodamine based selective turn-on sensing of picric acid, RSC Adv. 4 (2014) 30828–30831, https://doi.org/10.1039/C4RA02931C.

[62] S.A.A. Vandarkuzhali, S. Natarajan, S. Jeyabalan, G. Sivaraman, S. Singaravadivel, S. Muthusubramanian, B. Viswanathan, Pineapple peel-derived carbon dots: applications as sensor, molecular keypad lock, and memory device, ACS Omega 3 (2018) 12584–12592, https://doi.org/10.1021/acsomega.8b01146.

[63] S.K. Ko, X. Chen, J. Yoon, I. Shin, Zebrafish as a good vertebrate model for molecular imaging using fluorescent probes, Chem. Soc. Rev. 40 (2011) 2120–2130, https://doi.org/10.1039/C0CS00118J.